

# Nondipole Coulomb sub-barrier ionization dynamics and photon momentum sharing

Pei-Lun He,<sup>\*</sup> Michael Klaiber, Karen Z. Hatsagortsyan,<sup>†</sup> and Christoph H. Keitel  
*Max-Planck-Institut für Kernphysik, Saupfercheckweg 1, 69117 Heidelberg, Germany*  
(Dated: November 27, 2024)

The nondipole under-the-barrier dynamics of the electron during strong-field tunneling ionization is investigated, examining the role of the Coulomb field of the atomic core. The common analysis in the strong field approximation is consequently generalised to include the leading light-front non-dipole Coulomb corrections and demonstrates the counter-intuitive impact of the sub-barrier Coulomb field. Despite its attractive nature, the sub-barrier Coulomb field increases the photoelectron nondipole momentum shift along the laser propagation direction, involving a strong dependence on the laser field. The scaling of the effect with respect to the principal quantum number and angular momentum of the bound state is found. We demonstrate that the signature of Coulomb induced sub-barrier effects can be identified in the asymptotic photoelectron momentum distribution via a comparative study of the field-dependent longitudinal momentum shift for different atomic species with state-of-the-art experimental techniques of mid-infrared lasers.

Exchanges of photon's energy, momentum, and angular momentum with charged particles are fundamental building blocks of light-matter interactions. In the presence of an intense laser field, photon energy absorption can trigger nonlinear processes like high-order harmonic generation [1, 2], above-threshold ionization [3], and nonsequential double ionization [4]. Meanwhile, the angular momentum transfer from the laser beam is vital for generating vortex light [5, 6], polarized electrons [7, 8] and positrons [9], and nuclei vortices [10]. The absorption of the photon momentum has attracted considerable interest recently due to various breakthroughs in the experimental technique [11–18]. High precision measurements raised questions on how the absorbed photon momentum is partitioned between the photoelectron and the parent ion. The analysis relies on investigating the photoelectron momentum distribution (PMD) along the laser propagation direction. The coincidence measurement of the photoelectron and its parent ion provides a direct check of the momentum conservation law in the microscopic world [19].

It follows from energy and momentum conservation that in the simple-man model of tunneling ionization [2], when the electron appears in the continuum with a vanishing momentum due to a circularly polarized laser pulse, the total absorbed photon momentum is shared between the ion and electron as  $I_p/c$  and  $U_p/c$ , respectively [11, 20], where  $I_p$  is the ionization energy,  $U_p$  the ponderomotive potential, and  $c$  the speed of light. However, in deviation to the simple-man picture, there is a longitudinal momentum transfer to the electron during tunneling due to the laser Lorentz force  $\delta p_z \sim (\kappa/c)B_0\tau \sim I_p/c$ , where  $\kappa = \sqrt{2I_p}$  is the atomic velocity,  $\tau = \gamma/\omega$  the tunneling formation time,  $\gamma = \omega\kappa/E_0$  the Keldysh parameter,  $E_0$ ,  $B_0$ , and  $\omega$  are the laser electric, and magnetic fields, and its frequency, respectively. Atomic units are used throughout. Then, the most probable electron longitudinal momentum at the tunnel exit becomes  $I_p/(3c)$  [21],[14]. This is the case for a short-range atomic potential, when the electron begins the sub-barrier motion at the bound

state with a longitudinal momentum  $v_{zs} = -2I_p/(3c)$  [21, 22]. The Coulomb field of the atomic core reshapes the tunneling barrier and, consequently, the nondipole momentum shift due to the sub-barrier dynamics. The latter is also affected by the momentum distribution of the bound state, which contributes into the birth probability of the quantum orbit at  $v_{zs}$ .

The long-range character of the Coulomb field of the atomic core is known to play a key role in strong-field ionization. It enhances the tunneling probabilities [23–26]. In the continuum, it is responsible for the low-energy [27–33] and high-energy structures [34, 35] in the PMD and the interplay between nondipole and Coulomb effects [12, 13, 36–39]. The sub-barrier dynamics can induce specific effects in tunneling ionization [7, 8, 21, 40, 41]. For instance, the sub-barrier nonadiabatic dynamics results in a transverse momentum shift and polarized photoelectrons [7, 8]. The sub-barrier Coulomb effect can induce a phase shift of the quantum orbit [40], disturbing the holography pattern. However, there is yet no conclusion on how the under-the-barrier Coulomb action affects the nondipole momentum shift. While simulations via the time-dependent Schrödinger equation (TDSE) [42–44] and time-dependent Dirac equation [16] give accurately the final longitudinal momentum shift, they do not provide intuitive insight on the underlying sub-barrier dynamics.

In this Letter, we investigate the electron's sub-barrier nondipole dynamics in strong-field tunneling ionization within an enhanced analytical description including the role of the Coulomb field of the atomic core. The sub-barrier dynamics is described within the light-front [45] nondipole Coulomb-corrected strong-field approximation (SFA), while the continuum one via the light-front classical trajectory Monte Carlo (CTMC) simulation, disentangling the effect of the sub-barrier Coulomb action from that in the continuum. We found that the sub-barrier Coulomb effect induces an increase of the photoelectron nondipole longitudinal momentum shift, and discuss its counterintuitive physical origin. The dependence of the

Coulomb effect on the angular momentum of the bound state is analyzed. Finally, we discuss how the Coulomb effects in the sub-barrier nondipole momentum shift can be observed experimentally using mid-infrared laser fields.

Our description of the tunneling process is based on TDSE in the Göppert-Mayer gauge [46]

$$i \frac{\partial}{\partial t} \psi(\mathbf{x}, t) = \left[ \frac{1}{2} (\mathbf{p} + \mathbf{A}(\mathbf{x}, \eta))^2 + V(\mathbf{x}) - \phi(\mathbf{x}, \eta) \right] \psi(\mathbf{x}, t), \quad (1)$$

where  $V(\mathbf{x}) = -\frac{Z}{|\mathbf{x}|}$  is the Coulomb potential of the atomic core,  $A^\mu = (\phi, \mathbf{A})$  the laser four-vector potential in the Göppert-Mayer gauge, with  $\phi = -\mathbf{x} \cdot \mathbf{E}(\eta)$  and  $\mathbf{A}(\mathbf{x}, \eta) = \hat{\mathbf{z}}\phi/c$ ,  $\mathbf{E}(\eta) = E_0 [\hat{\mathbf{x}} \cos(\omega\eta) - \hat{\mathbf{y}} \sin(\omega\eta)] \exp\left(-2 \ln 2 \frac{\eta^2}{L^2}\right)$  the laser field of circular polarization with  $L = 4 T$  and  $T$  is the optical cycle, and with the light-front coordinate  $\eta = t - z/c$ . The Hamiltonian in Eq. (1) is accurate up to the  $1/c$  order, suitable in the considered parameter regime. The deviation from the fully relativistic theory [47–50] is given by  $I_p/c^2$  terms for the sub-barrier and  $U_p/c^2$  terms for the continuum dynamics. We apply light-front nondipole Coulomb-corrected SFA [51], which corresponds to the nondipole expansion of the relativistic theory [50]. The nondipole transition amplitude in the Göppert-Mayer gauge reads [59]:

$$M_{\mathbf{p}} = -i \int d\eta \frac{d^3\mathbf{x}}{(2\pi)^{3/2}} e^{-i \int_{\eta}^{\infty} d\eta' \frac{\frac{1}{2} \tilde{\mathbf{p}}(\eta')^2 + I_p}{1 - \frac{p_z}{c}}} \mathcal{F}_{\mathbf{C}}^*(\eta, \mathbf{x}) \quad (2)$$

$$\times (1 - \tilde{p}_z/c) e^{-i \tilde{\mathbf{p}}(\eta) \cdot \mathbf{x}} \cdot \mathbf{E}(\eta) \psi_{\kappa l m}(\mathbf{x}),$$

where  $\tilde{\mathbf{p}}(\eta) = (\mathbf{p}_\perp + \mathbf{A}_\perp(\eta), p_- - \frac{I_p}{c})$ , with  $p_- = p_z - \frac{p^2}{2c}$  is the light-front momentum,  $\mathbf{A}_\perp(\eta) \equiv -\int_{\infty}^{\eta} d\eta' \mathbf{E}(\eta')$ , and  $\psi_{\kappa l m}(\mathbf{x})$  is the bound state wave function. Note that  $p_z/c \approx p_-/c \approx \tilde{p}_z/c$  up to the  $1/c$  order. The use of the Göppert-Mayer gauge in the employed SFA is justified as it provides the accurate Coulomb corrected Perelomov-Popov-Terent'ev (PPT) ionization rate [23–25], which is well confirmed experimentally. The influence of the Coulomb field on the sub-barrier continuum electron is described by the Coulomb correction (CC) factor:

$$\mathcal{F}_{\mathbf{C}}(\eta, \mathbf{x}) = \exp \left\{ i \int_{\eta}^{\infty} d\eta' V(\mathbf{x}(\eta, \eta')) / \left( 1 - \frac{p_-}{c} \right) \right\}. \quad (3)$$

With saddle-point integration of Eq. (2), the differential ionization rate in the adiabatic regime is obtained [51]:

$$\Gamma^{(n,l,m)}(\eta, v_\perp, p_-) = \frac{\kappa}{\tilde{\kappa}} \frac{2^{2\nu+2} C_{\kappa l}^2 \kappa^{6\nu}}{\left(1 - \frac{p_-}{c}\right)^{2\nu} E(\eta)^{2\nu}} \quad (4)$$

$$\times |Y_{lm}(\tilde{\mathbf{p}}(\eta_s))|^2 \exp \left[ -\frac{2}{3} \frac{\tilde{\kappa}^3}{E(\eta)(1 - \frac{p_-}{c})} \right].$$

where  $(n, l, m)$  are the atomic quantum numbers (the angular momentum projection is determined with respect to the laser propagation axis),  $E(\eta) = |\mathbf{E}(\eta)|$ ,  $\tilde{\mathbf{p}}(\eta_s)$  is the

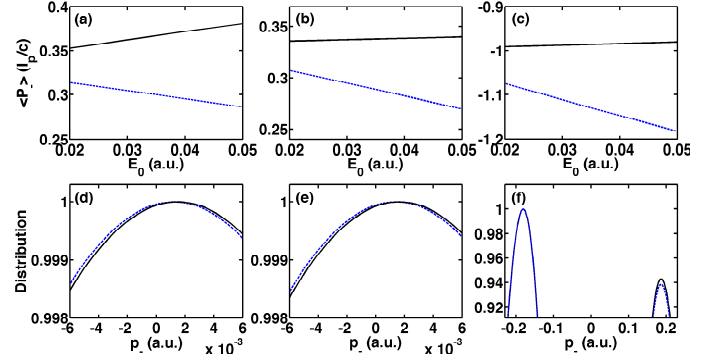


Figure 1. The sub-barrier Coulomb effect, neglecting the continuum influence, in the quasistatic regime: (a-c) The expectation value  $\langle p_- \rangle$  vs  $E_0$ ; (d-f) PMDs at the laser intensity  $I = 10^{14}$  W/cm $^2$ . The initial states are (a,d) hydrogen atom with quantum numbers (1, 0, 0), and argon atom (b,e) with (3, 1, 1), and (c,f) with (3, 1, 0). The solid-black line includes the sub-barrier Coulomb effect, while the dashed-blue line is the case of a short-range potential.

saddle-point momentum,  $\nu = Z/\kappa$  the effective principal quantum number,  $v_\perp$  the initial velocity component in the polarization plane,  $C_{\kappa l}^2 = \frac{2^{2\nu-2}}{\nu(\nu+l)!(\nu-l-1)!}$ , and  $\tilde{\kappa} = \sqrt{\kappa^2 + \tilde{p}_z^2 + v_\perp^2}$ .

To implement the light-front CTMC simulations, we sample over all possible ionization instants, tunneling exits, and initial momenta as initial conditions for the classic equation of motion

$$\frac{dQ}{d\eta} = \{Q, H\}, \quad \frac{dP}{d\eta} = \{P, H\}, \quad (5)$$

where  $\{A, B\}$  is the Poisson bracket, with the canonical coordinates  $Q = (x, y, z)$  and  $P = (p_x, p_y, p_-)$ . Trajectories are weighted by  $\Gamma^{(n,l,m)}$  of Eq. (4). Accurate to the  $1/c$  order, we have the classical light-front Hamiltonian

$$H = \frac{(\mathbf{p}_\perp + \mathbf{A}_\perp)^2 + (p_- + V/c)^2}{2 \left( 1 - \frac{p_- + V/c}{c} \right)} + V. \quad (6)$$

The tunneling exit  $\mathbf{x}^e = -\frac{I_p}{1 - p_-/c} \frac{\mathbf{E}(\eta)}{E(\eta)^2}$  is obtained by taking the real part of the complex trajectory [51].

Let us first discuss the sub-barrier Coulomb effect. Neglecting the Coulomb field effect in the continuum leads to the conservation of  $P = (p_x, p_y, p_-)$ . We plot the expectation value of  $p_-$  in Fig. 1. From Eq. (4), we derive  $\langle p_- \rangle$  for an  $s$ -state in the leading order correction of  $E_0/E_a$  [51]:

$$\langle p_- \rangle = \frac{I_p}{c} \left[ \frac{1}{3} + (2\nu - 1) \frac{E_0}{E_a} \right], \quad (7)$$

with the atomic field  $E_a = \kappa^3$ . Note that the leading  $I_p/(3c)$  term can be derived only employing the binding

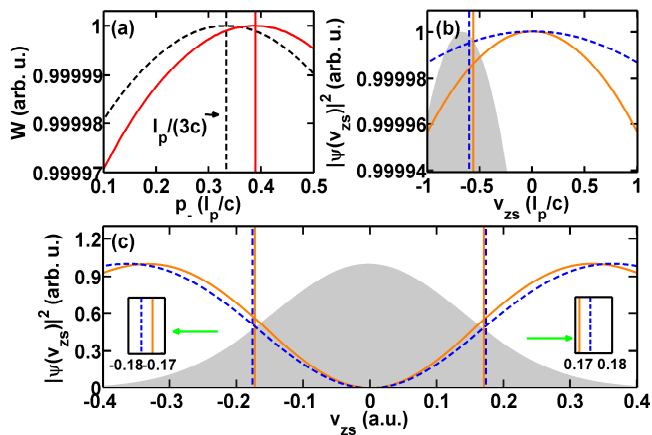


Figure 2. (a) The nondipole CC ionization window  $\mathcal{W}(p_-) \equiv |\mathcal{F}_C|^2 \exp\left[-\frac{2}{3} \frac{\tilde{\kappa}^3}{E(\eta)(1-p_-/c)}\right]$ : (solid-red) including the sub-barrier action, the peak is at  $p^m > I_p/(3c)$  (solid-red gridline), (dashed-black) neglecting the sub-barrier Coulomb correction,  $p^m \approx I_p/(3c)$  (dashed-black gridline). The bound state wave functions at the starting point of the tunneling trajectory  $x_s$ : (b) for  $(1, 0, 0)$  state, (c) for  $(3, 1, 0)$  state; the wave function for the zero-range potential (dashed-blue), and for the Coulomb case (solid-orange); the tunneling window  $\mathcal{W}$  is shadowed;  $E_0 = 0.04$  a.u. The gridlines in (b-c) indicate the peaks of  $\mathcal{W}(v_{zs})|\psi(x_s, y_s, v_{zs})|^2$  with (solid-orange), and without the sub-barrier CC (dashed-blue).

energy  $I_p$  and classical Lorentz sub-barrier dynamics in imaginary-time without any extra information about the binding potential and any time or spatial dependencies of the laser field, see Sec.IB.2 in [51]. Apart from the constant  $I_p/(3c)$  [14, 21, 42, 59], the sub-barrier Coulomb effect yields an increase in the momentum shift, despite the attractive nature of the parent ion, and induces a strong dependence on the laser field and the principal quantum number of the bound state [Fig. 1].

The active electrons of most rare gas atoms are in the  $p$ -state. For instance, the ionization of the argon atom is dominated by signals from  $(3, 1, \pm 1)$  orbits, while the nondipole shift for  $(3, 1, 0)$  is more distinctive:

$$\langle p_- \rangle = \frac{I_p}{c} \left[ -1 + (6\nu - 5) \frac{E_0}{E_a} \right]. \quad (8)$$

The physical origin of the Coulomb field effects for the nondipole sub-barrier dynamics is encoded in the exponent and the prefactor of the ionization amplitude of Eq. (2). The action contributed by the kinetic part, i.e.  $\frac{1}{2} \tilde{\mathbf{p}}(\eta')^2 + I_p$  of Eq. (2), gives the tunneling exponent in Eq. (4). Due to the laser magnetic field, the tunneling electron obtains a momentum in the laser propagation  $z$ -direction, which decreases the longitudinal tunneling energy and the tunneling probability, the latter being maximal at  $p^m = I_p/(3c)$  [21]. We can estimate the contribution of the Coulomb action by evaluating Eq. (3)

with quantum orbits starting at the saddle point of the SFA-matrix element  $\mathbf{x}_s$  [60]. The momentum shift due to the sub-barrier Coulomb action  $\mathcal{F}_C$  is evaluated by the  $\eta$ -integration from the saddle-time  $\eta_s$  to the exit time  $\eta_r = \text{Re } \eta_s$ . The sub-barrier Coulomb action  $\mathcal{F}_C$  contributes to the momentum shift, yielding a peak at  $p^m > I_p/(3c)$ , see Fig. 2(a). An essential sub-barrier CC for the nondipole momentum shift stems from matching the bound state wave function in the Coulomb field to the tunneling wave packet. The prefactor accounts for the probability of the quantum orbit, which originates at the bound state with the momentum  $v_{zs}$ . The width of the momentum space wave function  $\psi_{\kappa lm}(x_s, y_s, v_{zs})$  (in the mixed representation, at the starting point of the ionization  $x_s$ ) in the Coulomb field is narrower than that in the short-range potential, see Fig. 2(b). The most probable  $v_{zs}^m$  is the peak of the function:  $|\psi(x_s, y_s, v_{zs})|^2 \mathcal{W}(v_{zs})$ , which is indicated by the gridlines in Fig. 2 (b,c). The solid-orange grid line in (b) includes the sub-barrier CC and is closer to the origin (larger  $v_{zs}$ ), which yields an increase of the longitudinal momentum at the tunnel exit, as the total longitudinal momentum transfer from  $\mathbf{x}_s$  to  $\mathbf{x}^e$  is  $I_p/c$ .

The momentum shift and the corresponding CC depend essentially on the angular momentum of the bound state. We compare in Fig. 1 the expectation value of  $\langle p_- \rangle$  with and without CC for quantum numbers  $(1, 0, 0)$  (hydrogen) and  $(3, 1, 0)$ ,  $(3, 1, 1)$  (argon). There is a significant difference between  $s$ - and  $p$ -states. While the PMD of  $(1, 0, 0)$  and  $(3, 1, \pm 1)$  has only one peak, it has two peaks around  $\pm \sqrt{E_0/\kappa}$  for  $(3, 1, 0)$ , which originate from the momentum distribution of the initial bound state, see Fig. 2(c). In the dipole theory, the two peaks are equally probable and  $\langle p_- \rangle = 0$ . The center of the window  $\mathcal{W}$  is at

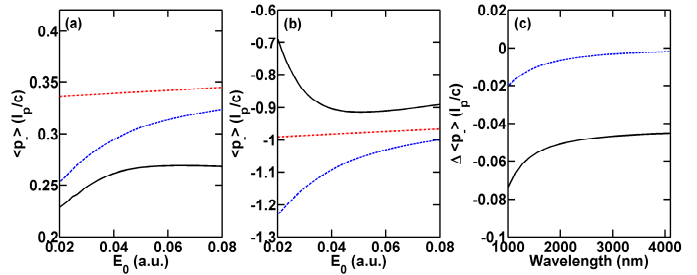


Figure 3. Asymptotic light-front momentum  $\langle p_- \rangle$  vs  $E_0$  when the initial states are an argon atom with quantum numbers (a)  $(3, 1, 1)$  and (b)  $(3, 1, 0)$ . The solid black lines include the continuum and the sub-barrier CC, the dashed-dotted red lines only the sub-barrier CC, and the dashed blue lines only the sub-barrier CC and nonadiabatic effects. (c) The contributions  $\Delta \langle p_- \rangle$  of the nonadiabatic effect (dashed-blue) and the continuum CC (solid-black) to  $\langle p_- \rangle$  vs the laser wavelength, for the laser intensity of  $10^{14}$  W/cm $^2$ .

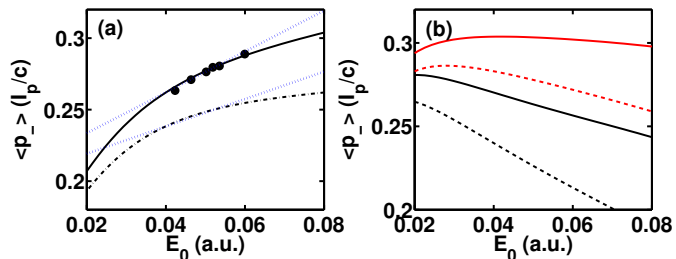


Figure 4. (a)  $\langle p_- \rangle$  vs  $E_0$  for the ground state hydrogen atom when the laser wavelength is 800 nm. Circles are results of TDSE simulations. Dotted blue lines are linear fittings of the curves. (b)  $\langle p_- \rangle$  vs  $E_0$  for Xe and  $\text{Xe}^+$  when the laser wavelength is 3000 nm. The solid lines include the full CC, while the dashed lines do not include the sub-barrier CC. The black lines are for Xe, and the red lines are for  $\text{Xe}^+$ .

$v_{zs} = -2I_p/(3c)$  in the nondipole theory. The asymmetry of the window with respect to the origin results in suppression of the probability of the positive peak with respect to the negative one, yielding a negative longitudinal momentum  $\langle p_- \rangle < 0$ . After accounting for the atomic Coulomb field, the peaks of the wave function become closer, which results in an increase of the PMD peaks. The sub-barrier CC for the right peak is larger [Fig. 1(f)], which leads to a decrease of  $\langle p_- \rangle$  by absolute value. Hence for the state  $(3, 1, 0)$ , the exponent of Eq. (4) prefers the peak  $p_- \approx -\sqrt{E_0/\kappa}$  due to the nondipole momentum shift  $I_p/c$ , while the prefactor prefers the peak  $p_- \approx \sqrt{E_0/\kappa}$  due to the sub-barrier Coulomb field effect.

Next let us discuss the role of the Coulomb field in the continuum and the nonadiabatic effect, see Fig. 3.  $P = (p_x, p_y, p_-)$  is no longer conserved and the momentum is reduced by absolute value as a result of the Coulomb momentum transfer mostly at the tunnel exit. For the states  $(3, 1, \pm 1)$  (argon) the continuum CC decreases the momentum shift, however, approximately maintaining the slope of the field dependence [51]. For a smaller electric field strength, the tunneling exit is farther away from the atomic core, while the photoelectron can stay a longer time around the nuclei. As a consequence,  $\langle p_- \rangle$  decreases in the absolute value, while the slope of the curve remains less affected. For the state  $(3, 1, 0)$ , the continuum CC reduces the momentum shift for the peak at  $p_- \approx \sqrt{E_0/\kappa}$  while increasing it for the peak at  $p_- \approx -\sqrt{E_0/\kappa}$ . The net result increases the total momentum shift. The qualitative behavior of the nonadiabatic corrections is similar (those without sub-barrier CC were considered in [61]). While the nonadiabatic effect decreases the absolute value of  $\langle p_- \rangle$ , it increases the slope of the field dependence. The contributions of the nonadiabatic and the continuum CC effects are calibrated via the difference of the momentum shift  $\Delta \langle p_- \rangle$ , calculated with and without these effects, see

Fig. 3(c). Both the continuum CC and the nonadiabatic effects are suppressed at longer laser wavelengths.

It is possible to detect the sub-barrier CC signal with the current experimental capabilities similar to Refs. [14, 15]. The momentum shift as well as the slopes of the field dependence are different after including the sub-barrier effect. In Fig. 4(a), we sample the laser intensity range  $10^{14} - 2 \times 10^{14}$  W/cm<sup>2</sup> for the linear fitting. We have carried out TDSE simulations based on the split-operator method, from which we obtain the scaling of the momentum shift as  $\langle p_- \rangle \sim 1.44 \pm 0.22 (E_0/E_a)(I_p/c)$ . After including both the nonadiabatic effect and Coulomb corrections, the light-front CTMC simulations yield  $\langle p_- \rangle \sim 1.42 \pm 0.02 (E_0/E_a)(I_p/c)$ . Without the sub-barrier CC, the CTMC simulation gives only  $\langle p_- \rangle \sim 0.96 \pm 0.02 (E_0/E_a)(I_p/c)$ . Thus, the sub-barrier Coulomb dynamics induces a quite strong field dependence in the nondipole longitudinal momentum shift (a large slope vs the laser field) partly distinguishable in an experiment.

Comparing atoms with different effective principal quantum numbers  $\nu$  provides another possibility to observe the sub-barrier CC, see Fig. 4(b). The qualitatively robust signature of the sub-barrier CC is the increase of  $\langle p_- \rangle \sim 2\nu \frac{E_0}{E_a} \frac{I_p}{c}$  with a higher effective principal quantum number of the active electron. For the ionization of Xe and  $\text{Xe}^+$  with quantum numbers  $(3, 1, 1)$ , we have  $\nu = 1.06$  and  $\nu = 1.60$ , respectively. The sub-barrier CC signal is robust against the average over the magnetic quantum numbers. Thus, the comparison of the longitudinal momentum shift and its dependence on the laser field for different atoms can unambiguously confirm the signature of the sub-barrier CC in an experiment. The longer laser wavelengths are more beneficial for the observation of the considered effects, as the masking effect of nonadiabaticity can be avoided at  $\gamma < 1$ , see Fig. 3(c), which shows an increase of the continuum CC due to nonadiabaticity at shorter wavelengths.

Concluding, after introducing the light-front non-dipole Coulomb-corrected theory, we reveal a counterintuitive role of the Coulomb field of the atomic core in nondipole sub-barrier dynamics, which increases the photoelectron nondipole momentum shift despite its attractive nature, with consequences for the momentum partition of the absorbed laser photons. We demonstrate, disentangling the sub-barrier and continuum effects, that the Coulomb sub-barrier signatures can be observed in the asymptotic momentum distribution with long-wavelength laser fields by measuring the characteristic slope of the field dependence of the average longitudinal momentum in different gas targets.

P.-L. H. acknowledges support via the prize of the Shanghai Jiao Tong University for outstanding graduate students. We thank Manfred Lein for a helpful comment regarding the effective principal quantum number.

- \* peilun@mpi-hd.mpg.de  
† k.hatsagortsyan@mpi-hd.mpg.de
- [1] A. L’Huillier and P. Balcou, High-order harmonic generation in rare gases with a 1-ps 1053-nm laser, *Phys. Rev. Lett.* **70**, 774 (1993).
  - [2] P. B. Corkum, Plasma perspective on strong field multiphoton ionization, *Phys. Rev. Lett.* **71**, 1994 (1993).
  - [3] P. Agostini, F. Fabre, G. Mainfray, G. Petite, and N. K. Rahman, Free-free transitions following six-photon ionization of xenon atoms, *Phys. Rev. Lett.* **42**, 1127 (1979).
  - [4] A. L’Huillier, L. A. Lompre, G. Mainfray, and C. Manus, Multiply charged ions induced by multiphoton absorption in rare gases at 0.53  $\mu\text{m}$ , *Phys. Rev. A* **27**, 2503 (1983).
  - [5] L. Marrucci, C. Manzo, and D. Paparo, Optical spin-to-orbital angular momentum conversion in inhomogeneous anisotropic media, *Phys. Rev. Lett.* **96**, 163905 (2006).
  - [6] Y.-Y. Chen, J.-X. Li, K. Z. Hatsagortsyan, and C. H. Keitel,  $\gamma$ -ray beams with large orbital angular momentum via nonlinear Compton scattering with radiation reaction, *Phys. Rev. Lett.* **121**, 074801 (2018).
  - [7] I. Barth and O. Smirnova, Nonadiabatic tunneling in circularly polarized laser fields: Physical picture and calculations, *Phys. Rev. A* **84**, 063415 (2011).
  - [8] A. Hartung, F. Morales, M. Kunitski, K. Henrichs, A. Laucke, M. Richter, T. Jahnke, A. Kalinin, M. Schöffler, L. P. H. Schmidt, *et al.*, Electron spin polarization in strong-field ionization of xenon atoms, *Nat. Photon.* **10**, 526 (2016).
  - [9] Y.-F. Li, Y.-Y. Chen, W.-M. Wang, and H.-S. Hu, Production of highly polarized positron beams via helicity transfer from polarized electrons in a strong laser field, *Phys. Rev. Lett.* **125**, 044802 (2020).
  - [10] Z. Chen, P.-L. He, and F. He, Spiral nuclear momentum distribution for the dissociation of  $\text{h}_2^+$  in a circularly polarized laser pulse, *Physical Review A* **101**, 033406 (2020).
  - [11] C. T. L. Smeenk, L. Arissian, B. Zhou, A. Mysyrowicz, D. M. Villeneuve, A. Staudte, and P. B. Corkum, Partitioning of the linear photon momentum in multiphoton ionization, *Phys. Rev. Lett.* **106**, 193002 (2011).
  - [12] A. Ludwig, J. Maurer, B. W. Mayer, C. R. Phillips, L. Gallmann, and U. Keller, Breakdown of the dipole approximation in strong-field ionization, *Phys. Rev. Lett.* **113**, 243001 (2014).
  - [13] J. Maurer, B. Willenberg, J. Daněk, B. W. Mayer, C. R. Phillips, L. Gallmann, M. Klaiber, K. Z. Hatsagortsyan, C. H. Keitel, and U. Keller, Probing the ionization wave packet and recollision dynamics with an elliptically polarized strong laser field in the nondipole regime, *Phys. Rev. A* **97**, 013404 (2018).
  - [14] A. Hartung, S. Eckart, S. Brennecke, J. Rist, D. Trabert, K. Fehre, M. Richter, H. Sann, S. Zeller, K. Henrichs, *et al.*, Magnetic fields alter strong-field ionization, *Nat. Phys.* **15**, 1222 (2019).
  - [15] B. Willenberg, J. Maurer, B. W. Mayer, and U. Keller, Sub-cycle time resolution of multi-photon momentum transfer in strong-field ionization, *Nature communications* **10**, 1 (2019).
  - [16] N. Haram, I. Ivanov, H. Xu, K. T. Kim, A. Atia-tul Noor, U. S. Sainadh, R. D. Glover, D. Chetty, I. V. Litvinyuk, and R. T. Sang, Relativistic nondipole effects in strong-field atomic ionization at moderate intensities, *Phys. Rev. Lett.* **123**, 093201 (2019).
  - [17] S. Grundmann, D. Trabert, K. Fehre, N. Strenger, A. Pier, L. Kaiser, M. Kircher, M. Weller, S. Eckart, L. P. H. Schmidt, F. Trinter, T. Jahnke, M. S. Schöffler, and R. Dörner, Zeptosecond birth time delay in molecular photoionization, *Science* **370**, 339 (2020).
  - [18] A. Hartung, S. Brennecke, K. Lin, D. Trabert, K. Fehre, J. Rist, M. S. Schöffler, T. Jahnke, L. P. H. Schmidt, M. Kunitski, M. Lein, R. Dörner, and S. Eckart, Electric nondipole effect in strong-field ionization, *Phys. Rev. Lett.* **126**, 053202 (2021).
  - [19] S. Grundmann, I. Kircher, M. and Vela-Perez, G. Nalin, D. Trabert, N. Anders, N. Melzer, J. Rist, A. Pier, N. Strenger, *et al.*, Observation of photoion backward emission in photoionization of He and  $\text{N}_2$ , *Phys. Rev. Lett.* **124**, 233201 (2020).
  - [20] D. Cricchio, E. Fiordilino, and K. Z. Hatsagortsyan, Momentum partition between constituents of exotic atoms during laser-induced tunneling ionization, *Phys. Rev. A* **92**, 023408 (2015).
  - [21] M. Klaiber, E. Yakaboylu, H. Bauke, K. Z. Hatsagortsyan, and C. H. Keitel, Under-the-barrier dynamics in laser-induced relativistic tunneling, *Phys. Rev. Lett.* **110**, 153004 (2013).
  - [22] E. Yakaboylu, M. Klaiber, H. Bauke, K. Z. Hatsagortsyan, and C. H. Keitel, Relativistic features and time delay of laser-induced tunnel ionization, *Phys. Rev. A* **88**, 063421 (2013).
  - [23] A. M. Perelomov, V. S. Popov, and M. V. Terent’ev, Ionization of atoms in an alternating electric field, *Sov. Phys. JETP* **23**, 924 (1966).
  - [24] A. M. Perelomov and V. S. Popov, Ionization of atoms in an alternating electric field. III, *Sov. Phys. JETP* **25**, 336 (1967).
  - [25] M. V. Ammosov, N. B. Delone, and V. P. Krainov, Tunnel ionization of complex atoms and of atomic ions in an alternating electromagnetic field, *Zh. Eksp. Teor. Fiz.* **91**, 2008 (1986).
  - [26] N. B. Delone and V. P. Krainov, Energy and angular electron spectra for the tunnel ionization of atoms by strong low-frequency radiation, *J. Opt. Soc. Am. B* **8**, 1207 (1991).
  - [27] C. I. Blaga, F. Catoire, P. Colosimo, G. G. Paulus, H. G. Muller, P. Agostini, and L. F. DiMauro, Strong-field photoionization revisited, *Nat. Phys.* **5**, 335 (2009).
  - [28] W. Quan, Z. Lin, M. Wu, H. Kang, H. Liu, X. Liu, J. Chen, J. Liu, X. T. He, S. G. Chen, *et al.*, Classical aspects in above-threshold ionization with a midinfrared strong laser field, *Phys. Rev. Lett.* **103**, 093001 (2009).
  - [29] H. Liu, Y. Liu, L. Fu, G. Xin, D. Ye, J. Liu, X. T. He, Y. Yang, X. Liu, Y. Deng, C. Wu, and Q. Gong, Low yield of near-zero-momentum electrons and partial atomic stabilization in strong-field tunneling ionization., *Phys. Rev. Lett.* **109**, 093001 (2012).
  - [30] B. Wolter, M. G. Pullen, M. Baudisch, M. Sclafani, M. Hemmer, A. Senftleben, C. D. Schröter, J. Ullrich, R. Moshhammer, and J. Biegert, Strong-field physics with mid-ir fields, *Phys. Rev. X* **5**, 021034 (2015).
  - [31] C. Liu and K. Z. Hatsagortsyan, Origin of unexpected low energy structure in photoelectron spectra induced by midinfrared strong laser fields, *Phys. Rev. Lett.* **105**, 113003 (2010).
  - [32] T.-M. Yan, S. V. Popruzhenko, M. J. J. Vrakking, and

- D. Bauer, Low-energy structures in strong field ionization revealed by quantum orbits, *Phys. Rev. Lett.* **105**, 253002 (2010).
- [33] A. Kästner, U. Saalman, and J. M. Rost, Electron-energy bunching in laser-driven soft recollisions, *Phys. Rev. Lett.* **108**, 033201 (2012).
- [34] T. Keil, S. V. Popruzhenko, and D. Bauer, Laser-driven recollisions under the coulomb barrier, *Phys. Rev. Lett.* **117**, 243003 (2016).
- [35] P.-L. He, M. Klaiber, K. Z. Hatsagortsyan, and C. H. Keitel, High-energy direct photoelectron spectroscopy in strong-field ionization, *Phys. Rev. A* **98**, 053428 (2018).
- [36] M. Førre, J. P. Hansen, L. Kocbach, S. Selstø, and L. B. Madsen, Nondipole ionization dynamics of atoms in superintense high-frequency attosecond pulses, *Phys. Rev. Lett.* **97**, 043601 (2006).
- [37] J. Daněk, M. Klaiber, K. Z. Hatsagortsyan, C. H. Keitel, B. Willenberg, J. Maurer, B. W. Mayer, C. R. Phillips, L. Gallmann, and U. Keller, Interplay between coulomb-focusing and non-dipole effects in strong-field ionization with elliptical polarization, *J. Phys. B* **51**, 114001 (2018).
- [38] J. Daněk, K. Z. Hatsagortsyan, and C. H. Keitel, Analytical approach to coulomb focusing in strong-field ionization. i. nondipole effects, *Physical Review A* **97**, 063409 (2018).
- [39] B. Willenberg, J. Maurer, U. Keller, J. Daněk, M. Klaiber, N. Teeny, K. Z. Hatsagortsyan, and C. H. Keitel, Holographic interferences in strong-field ionization beyond the dipole approximation: The influence of the peak and focal-volume-averaged laser intensities, *Phys. Rev. A* **100**, 033417 (2019).
- [40] T.-M. Yan and D. Bauer, Sub-barrier coulomb effects on the interference pattern in tunneling-ionization photoelectron spectra, *Phys. Rev. A* **86**, 053403 (2012).
- [41] M. Klaiber, K. Z. Hatsagortsyan, and C. H. Keitel, Under-the-tunneling-barrier recollisions in strong-field ionization, *Phys. Rev. Lett.* **120**, 013201 (2018).
- [42] S. Chelkowski, A. D. Bandrauk, and P. B. Corkum, Photon momentum sharing between an electron and an ion in photoionization: from one-photon (photoelectric effect) to multiphoton absorption, *Phys. Rev. Lett.* **113**, 263005 (2014).
- [43] S. Chelkowski, A. D. Bandrauk, and P. B. Corkum, Photon-momentum transfer in multiphoton ionization and in time-resolved holography with photoelectrons, *Phys. Rev. A* **92**, 051401 (2015).
- [44] S. Chelkowski, A. D. Bandrauk, and P. B. Corkum, Photon-momentum transfer in photoionization: From few photons to many, *Phys. Rev. A* **95**, 053402 (2017).
- [45] P. A. M. Dirac, Forms of relativistic dynamics, *Rev. Mod. Phys.* **21**, 392 (1949).
- [46] H. Reiss, Theoretical methods in quantum optics: S-matrix and Keldysh techniques for strong-field processes, *Prog. Quant. El.* **16**, 1 (1992).
- [47] V. S. Popov, V. D. Mur, and B. M. Karnakov, The imaginary-time method for relativistic problems, *Sov. Phys. JETP Lett.* **66**, 229 (1997).
- [48] V. D. Mur, B. M. Karnakov, and V. S. Popov, Relativistic version of the imaginary-time formalism, *Sov. Phys. JETP Lett.* **87**, 433 (1998).
- [49] N. Milosevic, V. P. Krainov, and T. Brabec, Semiclassical dirac theory of tunnel ionization, *Phys. Rev. Lett.* **89**, 193001 (2002).
- [50] M. Klaiber, E. Yakaboylu, and K. Z. Hatsagortsyan, Above-threshold ionization with highly charged ions in superstrong laser fields. ii. relativistic coulomb-corrected strong-field approximation, *Phys. Rev. A* **87**, 023418 (2013).
- [51] See the Supplemental Materials for the details, which includes Ref. [52-58].
- [52] V. S. Popov, Imaginary-time method in quantum mechanics and field theory, *Phys. Atom. Nucl.* **68**, 686 (2005).
- [53] J. I. Gersten and M. H. Mittleman, Eikonal theory of charged-particle scattering in the presence of a strong electromagnetic wave, *Phys. Rev. A* **12**, 1840 (1975).
- [54] O. Smirnova, M. Spanner, and M. Ivanov, Analytical solutions for strong field-driven atomic and molecular one- and two-electron continua and applications to strong-field problems, *Phys. Rev. A* **77**, 033407 (2008).
- [55] M. Klaiber, E. Yakaboylu, and K. Z. Hatsagortsyan, Above-threshold ionization with highly charged ions in superstrong laser fields. i. coulomb-corrected strong-field approximation, *Phys. Rev. A* **87**, 023417 (2013).
- [56] L. Keldysh, Ionization in the field of a strong electromagnetic wave, *Sov. Phys. JETP* **20**, 1307 (1965).
- [57] F. H. M. Faisal, Multiple absorption of laser photons by atoms, *J. Phys. B.* **6**, L89 (1973).
- [58] H. R. Reiss, Effect of an intense electromagnetic field on a weakly bound system, *Phys. Rev. A* **22**, 1786 (1980).
- [59] P.-L. He, D. Lao, and F. He, Strong field theories beyond dipole approximations in nonrelativistic regimes, *Phys. Rev. Lett.* **118**, 163203 (2017).
- [60] M. Klaiber, J. Daněk, E. Yakaboylu, K. Z. Hatsagortsyan, and C. H. Keitel, Strong-field ionization via a high-order coulomb-corrected strong-field approximation, *Physical Review A* **95**, 023403 (2017).
- [61] H. Ni, S. Brennecke, X. Gao, P.-L. He, S. Donsa, I. Brezinová, F. He, J. Wu, M. Lein, X.-M. Tong, and J. Burgdörfer, Theory of Subcycle Linear Momentum Transfer in Strong-Field Tunneling Ionization, *Phys. Rev. Lett.* **125**, 073202 (2020).